Role of Photolysis Frequency in Enhanced Selectivity and Yield for Controlled Bond Breaking in HOD

Manabendra Sarma and Manoj K. Mishra*

Department of Chemistry, Indian Institute of Technology, Bombay, Powai 400076, India

Received: December 21, 2007; Revised Manuscript Received: March 10, 2008

Quantum dynamical calculations on HOD subjected to different combinations of IR and UV pulses have been made to isolate field attributes which maximize selectivity and yield in the photodissociation of the desired O−H/O−D bond. Results from IR/UV pulse combinations which provide very high selectivity and/or yield are analyzed in detail by using population transfer, probability density flow, and flux variations to obtain microdynamic details favoring selectivity and yield. Results indicate that a 2727 cm^{-1} 50 fs Gaussian IR pulse in conjunction with a 46 062 cm^{-1} 50 fs Gaussian UV pulse with a time lag of ∼90 fs between the IR and UV pulses gives 79.1% flux in the H−O + D channel and 6.6% flux in the H + O−D channel, whereas a 3706 cm^{-1} 50 fs IR pulse in conjunction with a 51 090 cm^{-1} UV pulse gives 9.2% flux in the H−O + D channel and 82.1% flux in the H + O−D channel. A 2727 cm^{-1} 50 fs IR pulse in conjunction with a 40 062 cm^{-1} 50 fs UV pulse provides the greatest selectivity among the sampled field profiles with a flux branching ratio of H−O + D/H + O−D ≈ 487.8, and a 3706 cm^{-1} 50 fs IR pulse in conjunction with a 45090 cm^{-1} 50 fs UV pulse achieves a flux branching ratio of H + O−D/H−O + D ≈ 1354.8.

1. Introduction

Selective control of O−H and O−D bond dissociation in HOD has played an important role in the development of methods for laser-assisted control of chemical reactions,[1–7] and the HOD molecule has been a popular prototype for investigation of selective control of bond dissociation.[8–32] The H−OD (3706 cm^{-1}) and HO−D (2727 cm^{-1}) frequencies are well separated,[10,11,13,19,33] and it is therefore possible to prepare more or less pure O−H and O−D modes[10,11,13–19,21–23,26,28] which exclusively stretch the desired bond.[19] The first excited $\tilde{A}(^1B_1)$ surface of HOD is purely repulsive,[11,34–36] and UV-mediated deposition of the HOD molecule to appropriate region of the $\tilde{A}(^1B_1)$ surface has become a popular tool for selective control of bond dissociation in this system.[9–19,21–23,25–32] Selectivity in dissociation of the O−H bond has been demonstrated even without prior vibrational excitation of the O−H bond,[9–13,21,27,29–32] but in most cases, prior excitation of the O−H bond to ensure the deposition of the HOD molecule in the dissociative H + O−D channel on transition to the first excited repulsive $\tilde{A}(^1B_1)$ surface has been the more favored route.[9–11,13–19,23–26] In the case of selective dissociation of the O−D bond via transition to the repulsive first excited surface, prior excitation in the O−D stretch has been necessary.[11,13,19,21,22,28,30,31] The experimental and theoretical approaches for selective cleavage of the desired O−H/O−D bond in HOD are built around the prior localization of many quanta of vibrational excitation in these localized modes[9–11,13–19,21–26,28,30,31] to ensure that transfer to the upper repulsive $\tilde{A}(^1B_1)$ surface is localized in the desired dissociative channel.

Most such applications however have used a pure O−H/O−D overtone as the initial state,[10,11,13–19,21–23,26,28] and the role of the UV photolysis pulse has been limited to transferring the vibrationally excited molecule to the repulsive upper surface. As has been shown earlier[19] and will be seen in the results presented here, even a moderately intense IR pulse produces not a pure overtone but a linear combination of excited vibrational states, and non-δ-function-type UV pulses not only transfer population to the upper surface but induce a cross-talk between the surfaces with considerable influence on the dissociative outcome.[30–32] In the results presented here, it will be seen that under these more realistic conditions, there is an unmistakable inter-mode probability density flow, and a quantitative analysis of the dependence of selectivity and yield on field attributes which will facilitate a bypassing of this trans-modal flow can be most useful in achieving specific bond cleavage.

To the best of our knowledge, such an investigation of dependence of selectivity and yield on photolysis frequency and the microdynamical details facilitating their maximization has not been provided so far, and toward this end, we present a rigorous examination of dynamical details of selective control without any assumption of idealized conditions in this paper. It is our purpose to present an analysis of population transfer and probability density flows that result from exposure of the HOD molecule to combination of IR/UV pulses so as to elicit field attributes which facilitate both selectivity and yield without assuming a pure overtone as the initial state or ignoring the UV-pulse-induced cross-talk between the ground and excited surfaces. Also, the UV pulses used here are not ultrashort or δ-function type but have a temporal width that leads to a sufficiently narrow frequency bandwidth to ensure that mechanistic analysis based on excitation of individual vibrational levels remains feasible. Finally, results from the use of different IR/UV combinations are sifted to identify and bypass trans-modal flow to achieve (i) selective dissociation of O−H/O−D bonds with large yield, (ii) greater selectivity with some loss in yield, and (iii) almost complete selectivity at low yields. These results are also analyzed to see whether dynamical features that facilitate selectivity and yield can be isolated for further experimentation and understanding of control in more complicated systems. It will be seen that trans-modal flow manifests

* To whom correspondence should be addressed. E-mail: mmishra@iitb.ac.in. Fax: +91-22-2576-7152.

10.1021/jp711984t CCC: $40.75 © 2008 American Chemical Society
Published on Web 05/14/2008

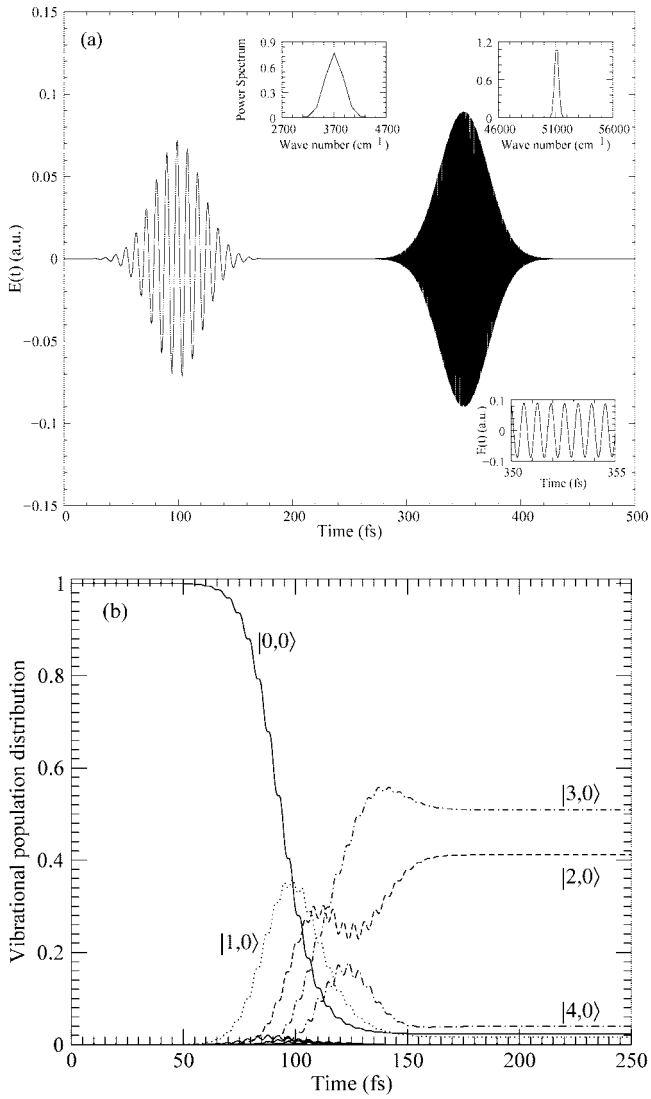

Figure 1. (a) IR and UV laser pulses with pulse profile $E(t) = A_0 a(t) \exp[-\gamma(t - t_0)^2] \cos(\omega t)$. For IR pulse, $A_0 = E_0 \cos\phi$ with $\phi = (\pi - \theta)/2$, $\theta = 104.52°$, $E_0 = 0.025$, and $a(t) = [(8\gamma t_l^2)/\pi]^{1/4}$ with fwhm $= [(4 \ln 2)/\gamma]^{1/2} = 50$ fs, $t_l = 250$ fs, $t_0^{ir} = 100$ fs, and $\omega_{ir} = 3706$ cm^{-1}. For the 50 fs UV laser pulse, $A_0 = 0.09$, $a(t) = 1$, $t_0^{uv} = 350$ fs, and $\omega_{uv} = 51\,090$ cm^{-1}. Power spectra for IR and UV pulses and more resolved UV field profile are presented as insets. (b) Vibrational population distribution from $|0, 0\rangle$ as the initial state under the influence of the IR pulse depicted in panel a.

itself even for this simple prototype with well separated bond frequencies, and the procedure for diminution of trans-modal flow adopted here could have more general utility.

The following section presents an outline of computational considerations and IR/UV field attributes. Section 3 provides a discussion of results, and a summary of the main observations concludes this paper.

2. Method

Following earlier work in this area,[10,11,13–19,21–23,26,28] our approach to selective control of HOD photodissociation proceeds with the use of an IR laser which produces a combination of pure O−H ($|m,0\rangle$, m quanta of excitation in the O−H bond)/ pure O−D ($|0, n\rangle$, n quanta of excitation in the O−D bond) vibrational levels to be subjected to a 50 fs UV laser pulse with frequencies enabling its transport to the first excited repulsive $\tilde{A}(^1B_1)$ surface with a time lag of ∼90 fs between the IR and

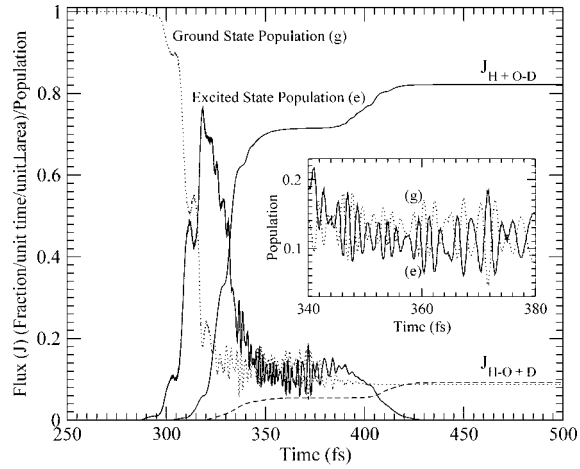

Figure 2. Ground- and excited-state populations and accumulated H + O−D and H−O + D flux from the vibrational population distribution shown in Figure 1b under the influence of the IR/UV pulses shown in Figure 1a.

UV pulses. In this IR/UV regime, the time evolution of nuclear motion is governed by[19,26]

$$i\hbar\frac{\partial}{\partial t}\begin{pmatrix}\Psi_g\\ \Psi_e\end{pmatrix} = \begin{pmatrix}\hat{H}_g + \hat{H}_{ir}(t) & \hat{H}_{uv}(t)\\ \hat{H}_{uv}(t) & \hat{H}_e\end{pmatrix}\begin{pmatrix}\Psi_g\\ \Psi_e\end{pmatrix} \quad (1)$$

where $\Psi_g = \Psi_g(r_1, r_2, t)$ and $\Psi_e = \Psi_e(r_1, r_2, t)$ are the ground- and excited-state wave functions, and r_1 and r_2 refer to O−H and O−D coordinates. The nuclear Hamiltonians for these two electronic states are expressed as $\hat{H}_g = \hat{T} + \hat{V}_g$ and $\hat{H}_e = \hat{T} + \hat{V}_e$, in which $\hat{T}$ and $\hat{H}_{uv}$ are detailed elsewhere.[19] $\hat{V}_g$ and $\hat{V}_e$ are obtained from refs 11 and 34–36, and eq. 1 is solved by using Ψ_g as ground vibrational state of the HOD and $\Psi_e = 0$, at $t = 0$. The IR−HOD interaction Hamiltonian $\hat{H}_{ir}(t)$ is the same as that used in earlier calculations.[19]

The vibrational eigenfunctions of HOD have been obtained from the two-dimensional Fourier grid Hamiltonian method.[37] In the time propagation of wave functions $\Psi_g(t)$ and $\Psi_e(t)$, the effect of kinetic energy operator on the wave function is evaluated by using a two-dimensional fast Fourier transform,[38] and the Lanczos scheme[39] has been used for time propagation. We have used a spatial grid spanning r_{O-H} /r_{O-D} bond lengths between 1 a_0 and 10 a_0 discretized on a mesh with 128 grid points. The step size in time propagation $\Delta t = 1$ au of time is ∼0.0242 fs, and the total propagation time is 500 fs.

The IR field form[19] is taken as $E(t) = A_0 a(t) \cos(\omega_{ir} t)$ where $A_0 = E_0 \cos\phi$ with $\phi = (\pi - \theta)/2$, $\theta = 104.52°$, and $a(t) = [(8\gamma t_l^2)/\pi]^{1/4} \exp[-\gamma(t - t_{ir})^2]$ with fwhm $= [(4 \ln 2)/\gamma]^{1/2}$. The frequency bandwidth of the IR pulse is ∼436 cm^{-1}, which permits mechanistic investigation in terms of individual vibrational levels. We have opted for a simple churn of the vibrational levels for O−H/O−D bonds by using appropriately powered IR field with carrier frequency tuned to the first excitation level−3706 cm^{-1} for $|1, 0\rangle$ mode with one quantum of excitation in the O−H mode or 2727 cm^{-1} for $|0, 1\rangle$ mode with one quantum of excitation in the O−D mode. The moderately high intensity of the IR laser leads to a combination $\sum_m c_m|m,0\rangle$ of pure O−H modes or a combination $\sum_n c_n|n,0\rangle$ of pure O−D modes. The maximum IR field amplitude for selective mixing of pure O−H modes is 0.13 GV/cm, corresponding to a maximum field intensity of 14 TW/cm^2. The maximum IR field amplitude for selective mixing of O−D modes is 0.26 GV/cm, corresponding to field intensity of 55 TW/cm^2. The IR field intensities have been chosen to produce maximum stretch in

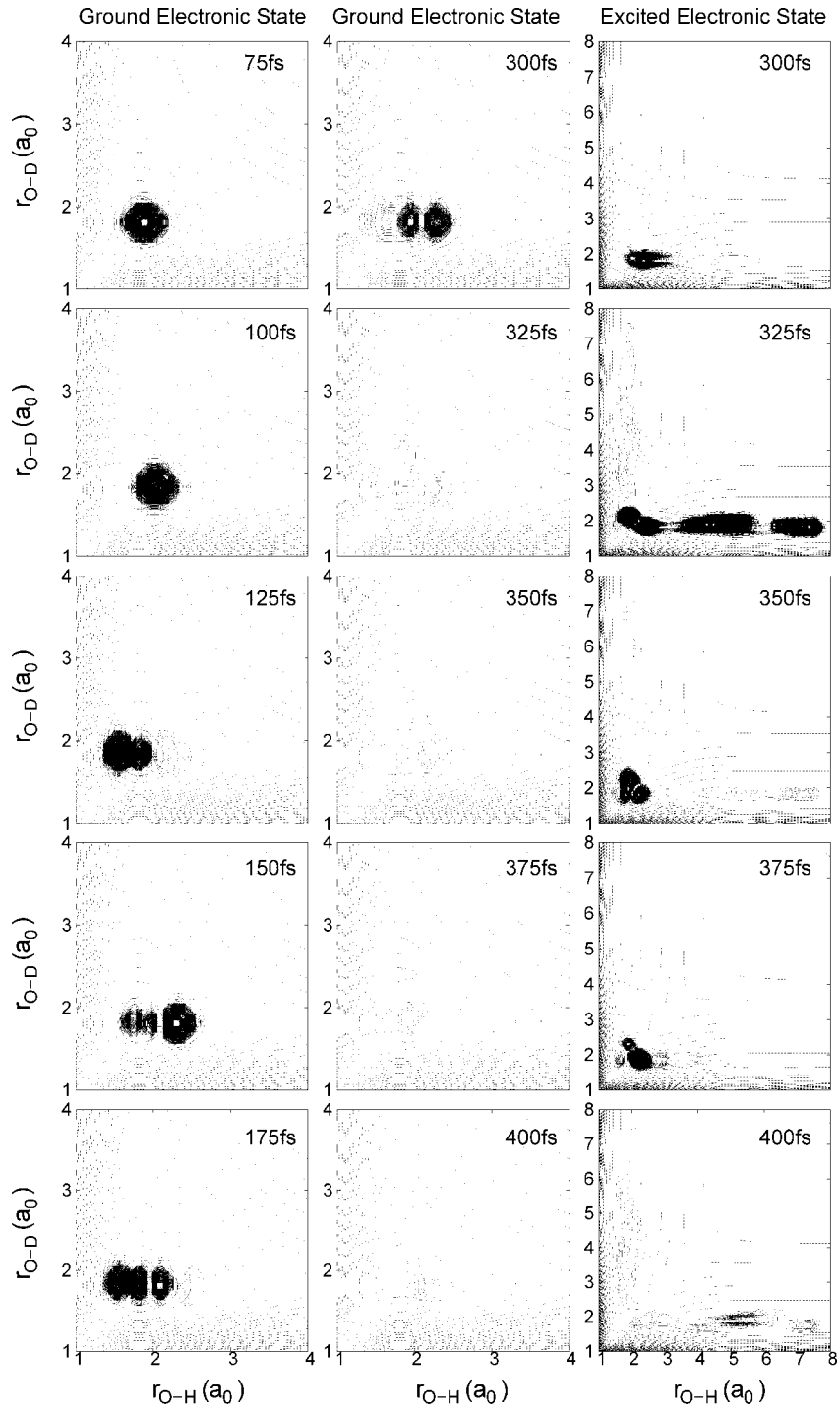

Figure 3. Time evolution of the $|0, 0\rangle$ state on the ground and excited surfaces for the IR/UV fields profiled in Figure 1a.

O−H/O−D bonds without any mix up of these pure bond modes. As in our previous investigations,[30–32] we have used a gaussian UV pulse[19] of the form $E(t) = 0.09a(t)\cos(\omega_{uv}t)$, where $a(t) = \exp[-\gamma(t - t_{uv})^2]$ with fwhm $= [(4 \ln 2)/\gamma]^{1/2} = 50$ fs. The maximum field amplitude for the UV pulse is 0.46 GV/cm, corresponding to field intensity of 178 TW/cm^2, and t_{uv} is fixed at 350 fs to permit a ∼90 fs time lag between switching off the IR field and onset of UV pulse so that it impacts a stable linear combination of O−H or of O−D modes. We have used a 90 fs delay between the IR and UV pulses to ensure that IR-induced vibrational population dynamics is completely insulated from the effect of the UV pulse. Other time delays are equally effective as long as the tails of the IR and UV pulses remain separated, and even a smaller time delay of 30 fs between the two pulses provides almost identical results. Similarly, we have chosen a UV pulse with 50 fs fwhm to ensure a sufficiently narrow frequency bandwidth. Although this bandwidth can be lowered further by increasing the UV pulse width, an increase in temporal width of the UV pulse changes the cross-talk-induced population transfer dynamics[32] between the ground and excited states. Longer UV pulses lead to some dephasing of the initial state prepared by the IR pulse, which can affect both selectivity and yield. The choice of UV pulse fwhm should therefore be calibrated accordingly.

As mentioned previously, unlike in earlier attempts involving solution of two surface time-dependent Schrödinger equa-

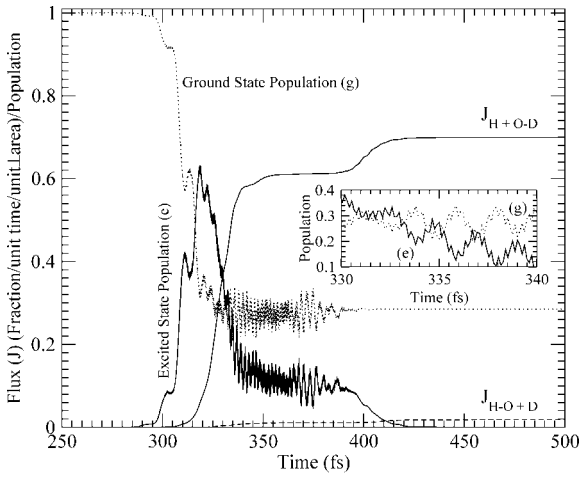

Figure 4. Same as Figure 2 except $\omega_{uv} = 49\,090$ cm^{-1}.

tions[19,21,26] for H−O−D, the pulse shapes utilized here have sufficiently narrow (∼446 cm^{-1}) frequency bandwidth (see Figures 1a and 8a) to ensure that mechanistic analysis based on excitation of individual vibrational levels remains feasible. We have used the same UV field amplitude as that in our earlier work, with resulting intensity that may be high enough to induce ionization. The IR field intensity is also somewhat high but is still lower than that employed in similar investigations of HOD, for example, 50 TW/cm^2 IR pulse in ref 19 and ∼600 TW/cm^2 IR pulse in ref 26. Results not tabulated here, however, show that substantial selectivity with reasonable yield may also be obtained by using IR and UV pulses of considerably lower intensities. The choice of IR and UV pulse intensity could therefore be altered to suit the selectivity/yield demand.

The time-integrated total flux in the competing channels, H + O−D ← H−O−D → H−O + D, is given by[30]

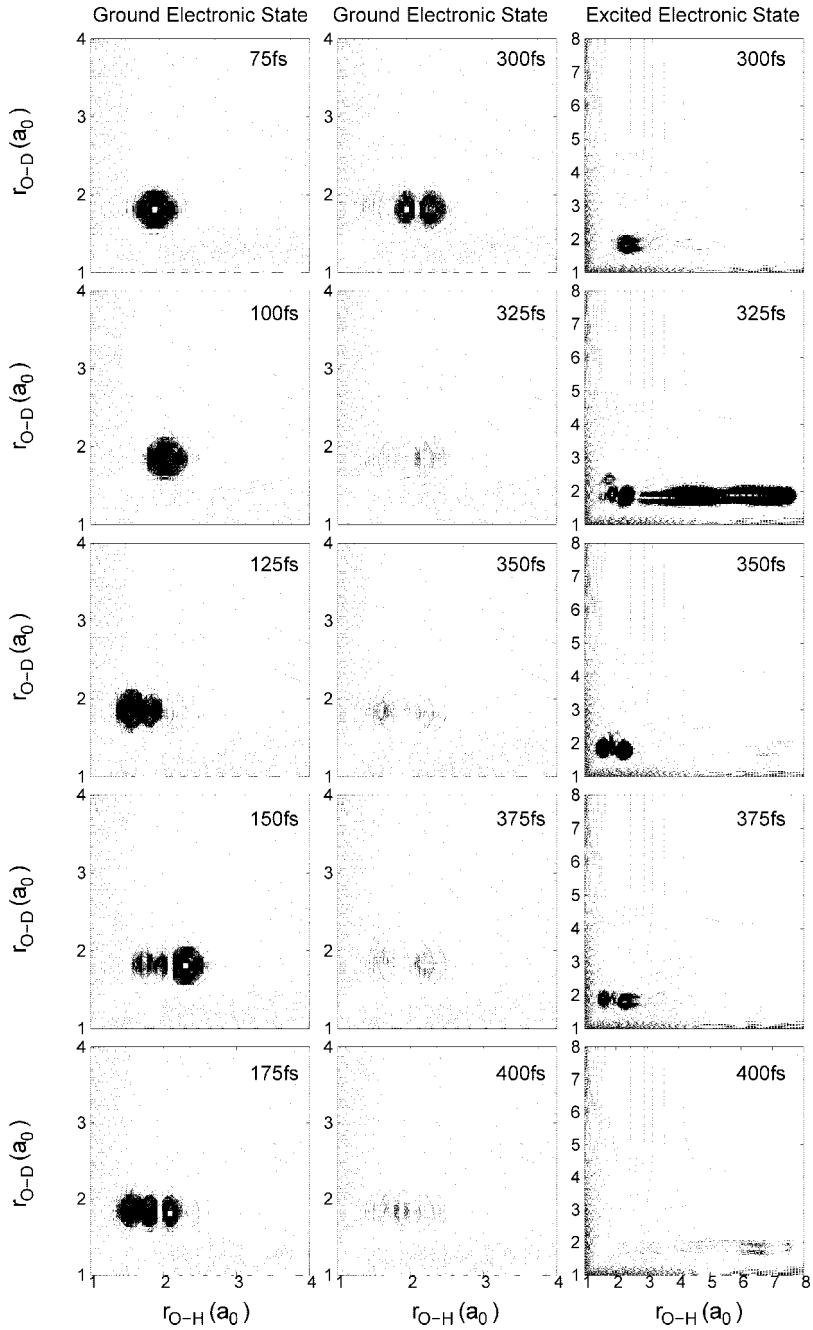

Figure 5. Same as Figure 3 except $\omega_{uv} = 49\,090$ cm^{-1}.

$$J_{H+O-D} = \int_0^{r_{2d}} \int_0^T \Psi^*(r_1, r_2, t)(\hat{j}_1 + \frac{\mu_2 \cos\theta}{m_0}\hat{j}_2) \times \Psi(r_1, r_2, t)\, dr_2\, dt \quad (2)$$

and

$$J_{H-O+D} = \int_0^{r_{1d}} \int_0^T \Psi^*(r_1, r_2, t)(\hat{j}_2 + \frac{\mu_1 \cos\theta}{m_0}\hat{j}_1) \times \Psi(r_1, r_2, t)\, dr_1\, dt \quad (3)$$

where $\hat{j}_i$ is the flux operator in the ith channel, defined as $\hat{j}_i = [1/(2\mu_i)][\hat{p}_i\delta(r_i - r_i^d) + \delta(r_i - r_i^d)\hat{p}_i]$. μ_i, $\hat{p}_i$, and r_i^d are the reduced mass, the momentum operator, and a grid point in the asymptotic region of the ith channel, respectively. The ground vibrational state of the molecule is our initial condition, and the flux in H+O−D/H−O+D channels are evaluated along asymptotic cuts at $r_{O-H} = r_{O-D} = 7.5a_0$. An absorbing optical potential is used to avoid unphysical reflection from the edges.

3. Results and Discussion

There is a kinematic bias favoring preferential dissociation of the O−H bond, and successful selective dissociation of this bond[9–19,21,23–27,29–32] has been the original precursor for the prototypical status of HOD in various approaches to selective control. A careful analysis of the microdynamical details arising from exposure of HOD to IR pulses which produce localized O−H excitations and the role of the photolyzing UV pulse frequency in selective dissociation of this bond is detailed in Figures 1–7.

The IR and UV pulses with their power spectrum are depicted in Figure 1a, and the resulting vibrational mix is shown in Figure 1b. As can be seen in Figure 1b, there is a stable combination of pure O−H modes with maximum population in the $|3, 0\rangle$ mode. This combination has sufficient prior stretch in the O−H bond, and results from subjecting this combination to UV pulses with different frequencies are displayed in Figures 2–7 and collected in Table 1. The flux values of Table 1 isolate the UV pulse with a frequency of 51 090 cm^{-1} to be most effective which incidentally will provide sufficient energy to place the HOD molecule with three quanta of excitation in the O−H mode—the dominant component of the linear combination resulting from the IR churn—just above the saddle point of the upper repulsive surface, and details of the population-transfer dynamics and dissociative flux in the H + O−D and H−O + D channels are shown in Figures 2 and 3. Results of Figure 2 show that as soon as the UV pulse begins to build sufficient power around 300 fs, there is a quick transfer of population to the excited surface which reaches a maximum by 325 fs. The excited upper surface being repulsive, the population in the excited state begins to flow almost simultaneously, and because of the prior stretching of the O−H bond on the ground surface, flux builds up in the H + O−D channel, with ~72% dissociation of the O−H bond being achieved within next 25 fs. The final flux of 82% in the H + O−D channel is achieved once the UV field switches off at 420 fs, shutting off the cross-talk between the ground and excited surfaces. There is no further dumping from the excited surface, and this allows for flushing of the population on the excited surface into the competing channels, as seen from a kick in both the H + O−D and H−O + D flux values around 400 fs.

The localization of vibrational excitation in the O−H bond is clearly seen in the 75−175 fs probability density plots of Figure 3, where gradual transformation of the $|0, 0\rangle$ ground vibrational state into the linear combination of pure O−H modes is easily seen. This linear combination resulting from the vibrational churn retains its shape until the UV field comes into play with sufficient power at 300 fs, and as can be seen in the probability density plots on the excited surface, the role of this prior vibrational excitation in engineering a favored flow into the H + O−D channel of the excited surface is quite effective indeed. It is also seen that unlike what has been assumed in some earlier analyses,[9,11,13,28] not only is a small wedge of the ground-state probability density accessible at the pulse frequency transferred to the upper surface, but there is a more or less complete transfer of the ground-state population to the upper surface, which ensures selectivity with substantial yield as seen in Table 1. The trans-modal flow into the H−O + D channel is seen to be initiated by the cross-talk between the two surfaces induced by the UV pulse from 325 fs onward with non-negligible amplitude in the O−D mode as well, on both the ground and the excited surfaces. Flow in the H−O + D channel of the excited surface is seen from 350 fs onward with a kick

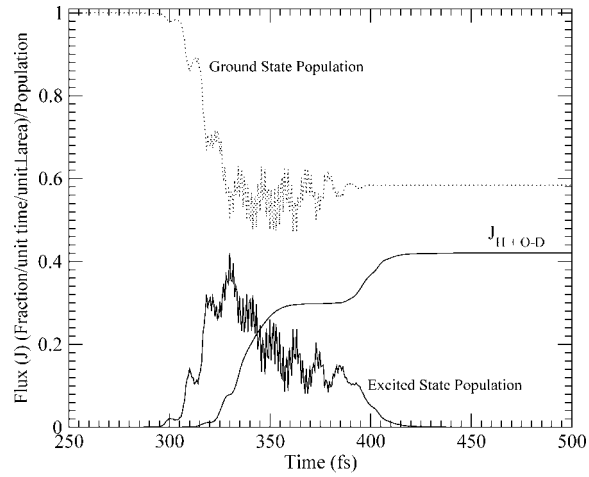

Figure 6. Same as Figures 2 and 4 except $\omega_{uv} = 45\,090$ cm^{-1}.

TABLE 1: Photodissociation Flux and Branching Ratio for Local O−H Modes under the Influence of the Field Profile Shown in Figure 1a

UV frequency, ω_{uv} (cm^{-1})	H + O−D flux	H−O + D flux	H + O−D/H−O + D flux ratio
59090	0.73	0.17	4.29
57090	0.73	0.14	5.21
55090	0.71	0.17	4.18
53090	0.79	0.11	7.19
51090	0.82	9.21×10^{-2}	8.90
49090	0.70	1.86×10^{-2}	37.63
47090	0.55	5.88×10^{-3}	94.82
45090	0.42	3.10×10^{-4}	1354.84
43090	0.12	2.00×10^{-5}	6000.00

TABLE 2: Photodissociation Flux and Branching Ratio for Local O−D Modes under the Influence of the Field Profile Shown in Figure 8a

UV frequency, ω_{uv} (cm^{-1})	H + O−D flux	H−O + D flux	H−O + D/H + O−D flux ratio
54062	0.25	0.64	2.56
52062	0.26	0.64	2.46
50062	0.19	0.70	3.68
48062	0.15	0.76	5.07
46062	6.57×10^{-2}	0.79	12.02
44062	8.97×10^{-3}	0.75	83.61
42062	3.09×10^{-3}	0.41	132.62
40062	4.10×10^{-4}	0.20	487.80
38062	1.20×10^{-4}	4.50×10^{-2}	375.00

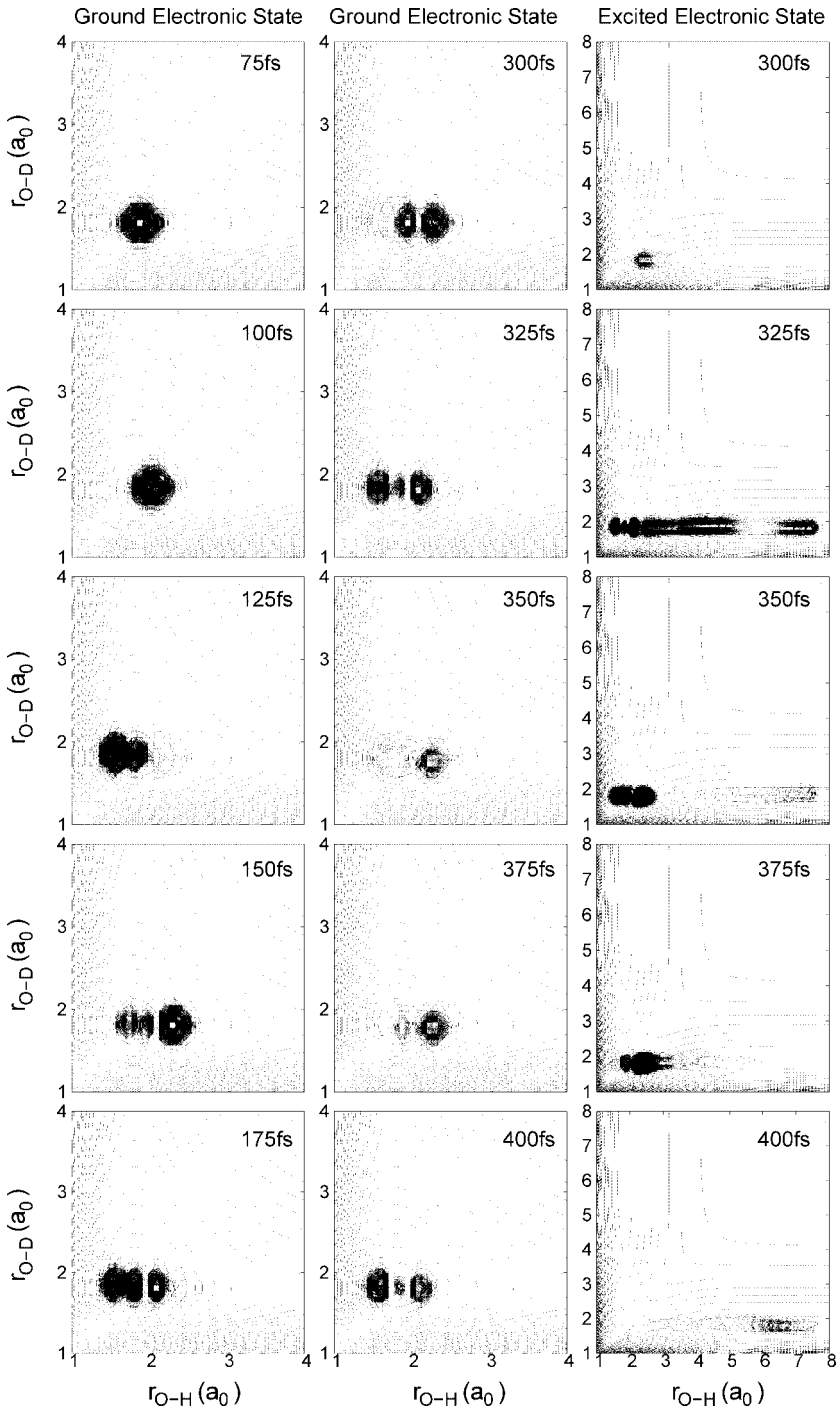

Figure 7. Same as Figures 3 and 5 except $\omega_{uv} = 45\,090\ cm^{-1}$.

at 400 fs as remarked earlier. The trans-modal flow into the H−O + D channel from 350 fs onward, even in this simple case with well separated bond frequencies, is difficult to miss.

A way around the trans-modal flow into the H−O + D channel is suggested by the lower frequency results of Table 1, where at 49 090 cm^{-1} we observe a 4-fold increase in branching ratio with only a 12% reduction of the H + O−D yield. The dynamical details are explored in Figures 4 and 5. At the lower UV frequency of 49 090 cm^{-1}, the temporal features are similar, and the time frame for population and flux build up is similar to that seen earlier in Figure 2; however, the excitation profile is different, and although the cross-talk between the two surfaces is somewhat more intense, the extent of population transfer is smaller at all times, with 29% of the population remaining untransferred in the ground state at the end of the UV pulse. The smaller UV frequency, however, also leads to a deposition of the population on the upper surface below the saddle-point barrier with insufficient energy to cross the saddle point. As a result, there is a much larger probability density on the ground surface in the 300−400 fs regime, and only a very small leakage into the H−O + D channel of the upper surface in the 350−375 fs interval. The prior stretching of O−H bond in conjunction with a UV pulse of frequency that is lower than that required to cross the excited-state saddle point results in a probability density profile that facilitates deposition in the H + O−D channel on the upper surface and the lower-frequency (energy) UV pulse prevents its leakage across the saddle-point barrier. We therefore see a confirmation of the earlier suggestions[11,13]

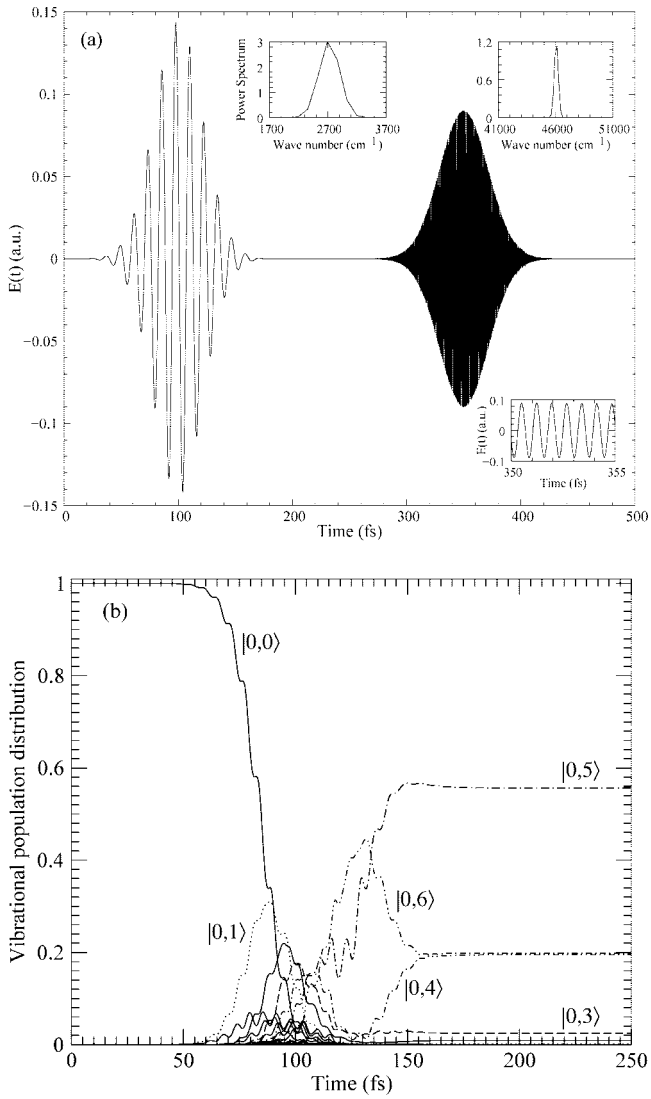

Figure 8. Same as Figure 1 except $E_0 = 0.05$, $\omega_{ir} = 2727$ cm^{-1}, and $\omega_{uv} = 46\,062$ cm^{-1}.

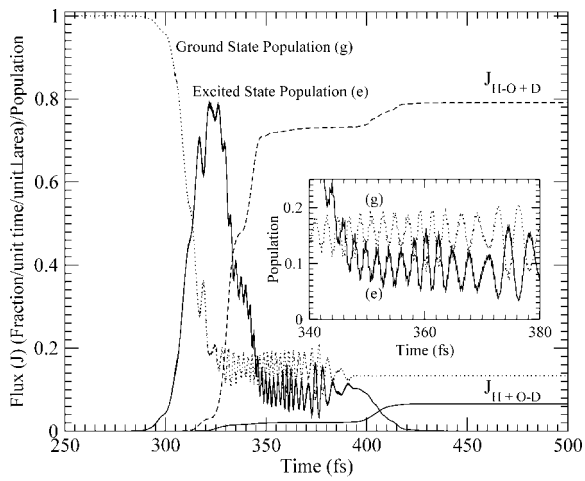

Figure 9. Same as Figures 2, 4, and 6 except that the IR/UV combination is the one presented in Figure 8.

for selective control to be essentially an instrument for bypassing trans-modal flow into the H−O + D channel, as shown in detail in the 300−400 fs probability density flow plots of Figure 5. There is ∼12% loss of yield in the H + O−D channel, but flux in the H−O + D channel is reduced to a mere 1.9%, providing very reasonable yield in O−H dissociation with great selectivity as well.

A further reduction of the UV frequency by 4000 cm^{-1} to 45 090 cm^{-1} leads to 42% flux in the H + O−D channel, with near zero flux in the H−O + D channel and a branching ratio of 1355 (see Table 1). The reason for this can be seen in Figures 6 and 7, where a much smaller population transfer to the excited state coupled with much lower excitation energy (UV frequency) keeps the probability density values high on the ground surface, and the population transferred to the excited surface is locked into the H + O−D channel with complete bypassing of trans-modal flow in the H−O + D channel at all times.

Further lowering of the UV frequency makes the UV pulse off-resonance vis-à-vis the excited surface with insignificant overall dissociation (see Table 1). It can also be seen from Table 1 that as the UV frequency values go beyond 51 090 cm^{-1}, the population transfer on the upper surface will be above the saddle-point barrier, and as expected, there is a loss in selectivity even with this combination of pure O−H modes.

The IR and UV pulses employed for selective control of O−D dissociation with their power spectrum are depicted in Figure 8a, and the resulting vibrational mix is shown in Figure 8b. As can be seen in Figure 8b, there is a stable combination of pure O−D modes with maximum population in the $|0, 5\rangle$ mode. This combination has sufficient prior stretch in the O−D bond, and results from subjecting this combination to UV pulses with different frequencies are displayed in Figures 9–14 and collected in Table 2. The flux values in Table 2 isolate the UV pulse with a frequency of 46 062 cm^{-1} to be most effective which incidentally will provide sufficient energy to place the HOD molecule with five quanta of excitation in the O−D mode—the dominant component of the linear combination resulting from the IR churn—just above the saddle point of the upper repulsive surface, and details of the population-transfer dynamics and dissociative flux in the H−O + D and H + O−D channels are shown in Figures 9 and 10. Results of Figure 9 show that as soon as the UV pulse begins to build sufficient power around 300 fs, there is quick transfer of population to the excited surface which reaches a maximum by 350 fs. The excited upper surface being repulsive, the population in the excited state begins to flow almost simultaneously, and because of the prior stretching of O−D bond on the ground surface, flux builds up in the H−O + D channel with ∼72% dissociation of the O−D bond being achieved within the next 10 fs. The final flux of 79% in the H−O + D channel is achieved once the UV field switches off at 420 fs, shutting off the cross-talk between the ground and excited surfaces. There is no further dumping from the excited surface, and this allows for flushing of population on the excited surface into the competing channels as seen once again, from a kick in both the H−O + D and H + O−D flux values around 400 fs.

The gradual build up of localized excitations in the O−D bond is depicted in the 75−175 fs probability density plots of Figure 10, where gradual transformation of the $|0, 0\rangle$ ground vibrational state into the linear combination of pure O−D modes is easily seen. This linear combination resulting from the vibrational churn retains its shape until the UV field comes into play with sufficient power at 300 fs, and as can be seen in the probability density plots on the excited surface, the role of this vibrational excitation in engineering a favored flow into the H−O + D channel of the excited surface is quite effective and in line with results discussed earlier for selective control of O−H bond dissociation. It is also seen that unlike what has been

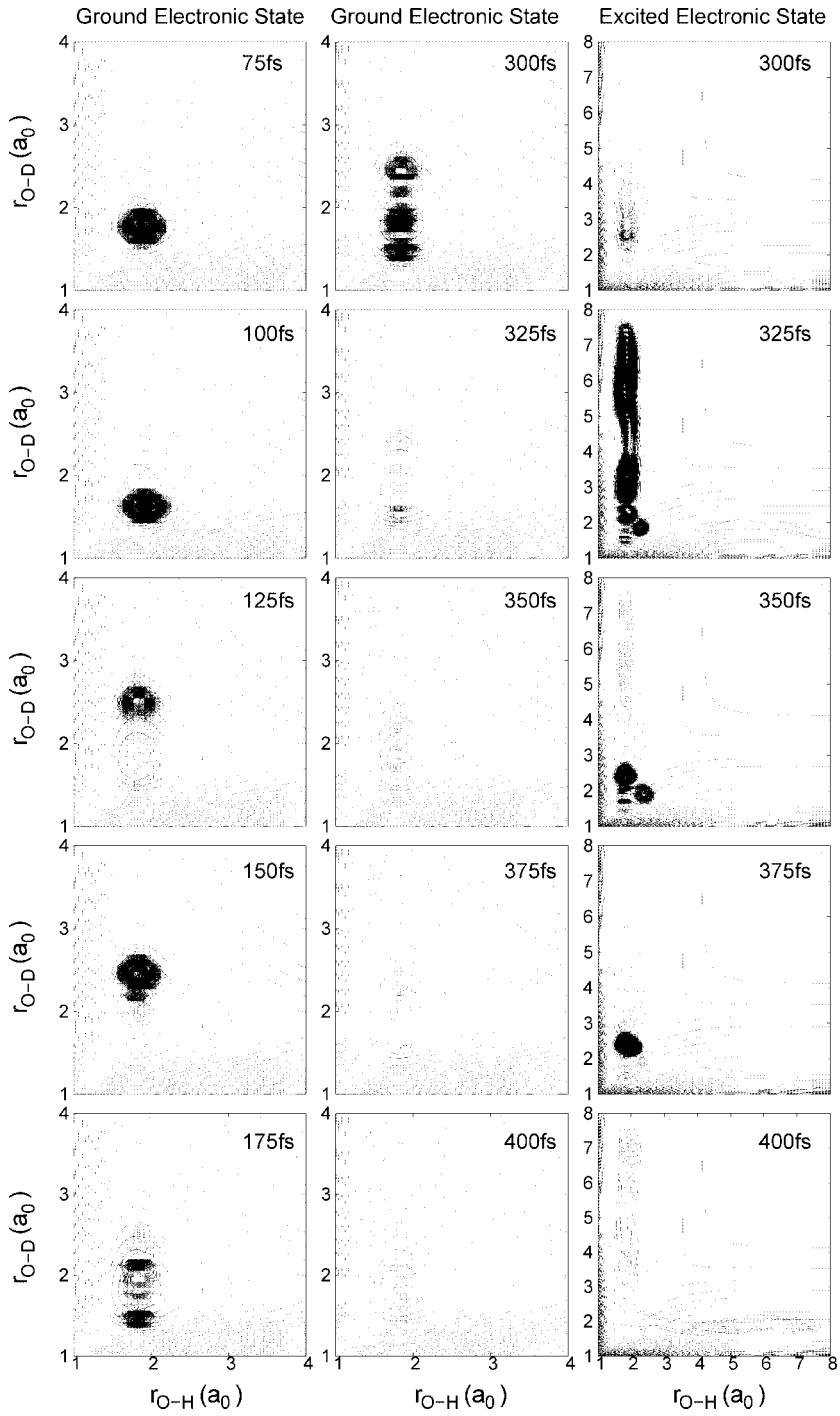

Figure 10. Same as Figures 3, 5, and 7 except that the IR/UV combination is the one presented in Figure 8.

assumed in some earlier analyses,[9,11,13,28] once again, not only is a small wedge of the ground-state probability density accessible at the pulse frequency transferred to the upper surface, but there is a more or less complete transfer of the ground-state population to the upper surface, which is required for ensuring selectivity with substantial yield as seen in Table 2. On the ground surface, the cross-talk between the two surfaces induced by the UV pulse leads to a small amplitude in the O−H mode as well at 350 fs, and a small flow in the H + O−D channel of the excited surface is seen from 350 fs onward with a kick at 400 fs as remarked earlier. Trans-modal flow from 350 fs onward, even in this simple case with well separated bond frequencies, is similar to that seen earlier.

The scheme for successfully circumscribing trans-modal flow in selective dissociation of O−H bond is confirmed by the lower frequency results of Table 2, where at 44 062 cm^{-1} we observe a 7-fold increase in branching ratio with only a 4% reduction of the H−O + D yield. The dynamical details are explored in Figures 11 and 12. At the lower UV frequency of 44 062 cm^{-1}, the time frame for population and flux build up is similar to that seen earlier in Figure 9, but the excitation profile is different, and although the cross-talk between the two surfaces is somewhat more intense, the extent of population transfer is smaller at all times, with 24% of the population remaining untransferred in the ground state at the end of the UV pulse. The smaller UV frequency, however, also leads to a deposition of the population on the upper surface below the saddle-point barrier with insufficient energy to cross the saddle point. As a result, there is a much larger probability density on the ground surface in the 300−400 fs regime and only a very small leakage

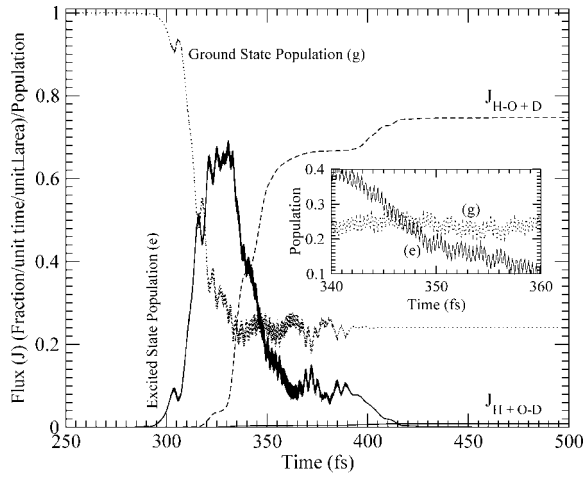

Figure 11. Same as Figure 9 except $\omega_{uv} = 44\,062$ cm^{-1}.

into the H + O−D channel of the upper surface in the 350−375 fs interval. The prior stretching of the O−D bond results in a probability density profile that facilitates deposition in the H−O + D channel on the upper surface, and the lower frequency (energy) UV pulse prevents its leakage across the saddle-point barrier. We see a confirmation of the selective O−H dissociation scenario in full detail. There is a 4% loss of yield in the H−O + D channel, but flux in the H + O−D channel is reduced to a mere 0.9%, providing very reasonable yield in O−D dissociation with great selectivity as well.

A further reduction of the UV frequency by 4000 cm^{-1} to 40 062 cm^{-1} leads to ∼20% flux in the H−O + D channel with near zero flux in the H + O−D channel and a branching ratio of 488 (see Table 2). The reason for this can be seen in Figures 13 and 14, where a much smaller population transfer to the excited state coupled with a much lower excitation energy (frequency) keeps the probability density values high on the

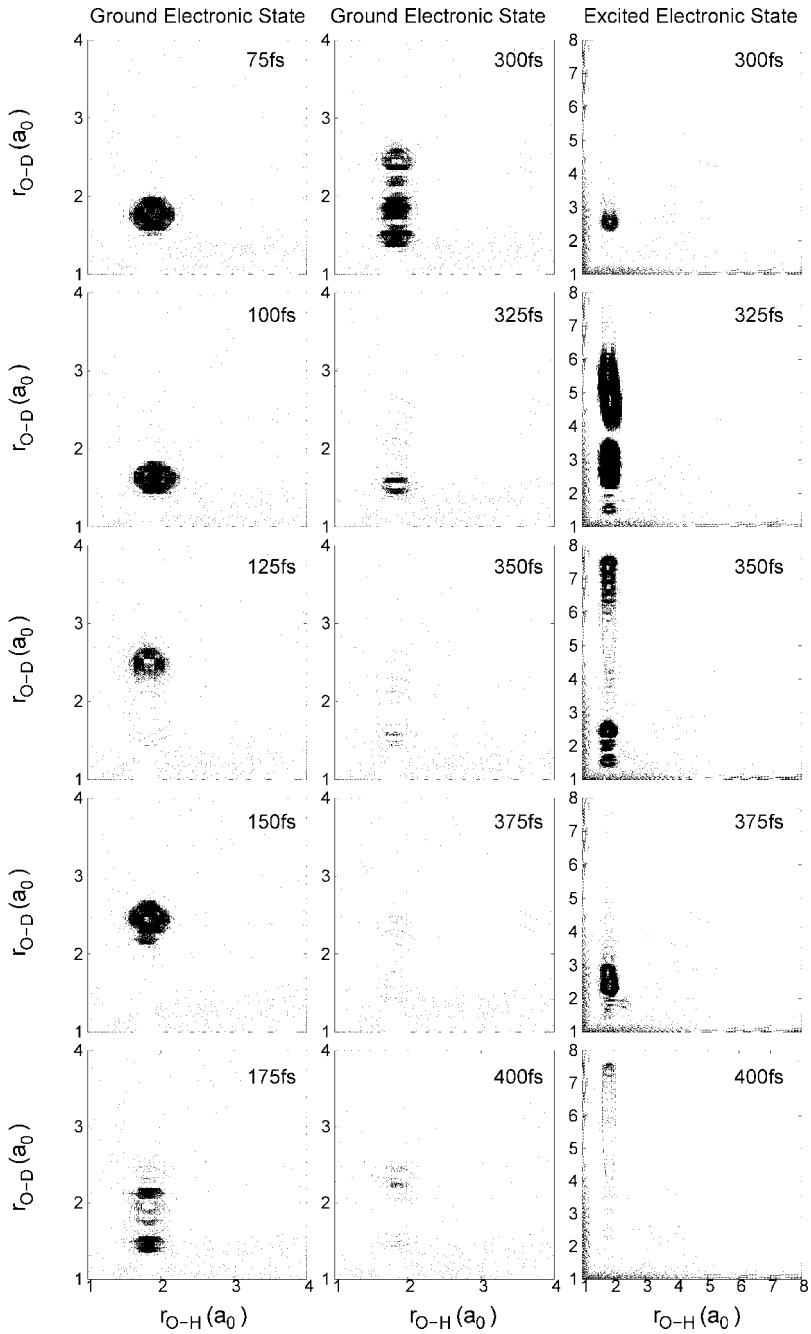

Figure 12. Same as Figure 10 except $\omega_{uv} = 44\,062$ cm^{-1}.

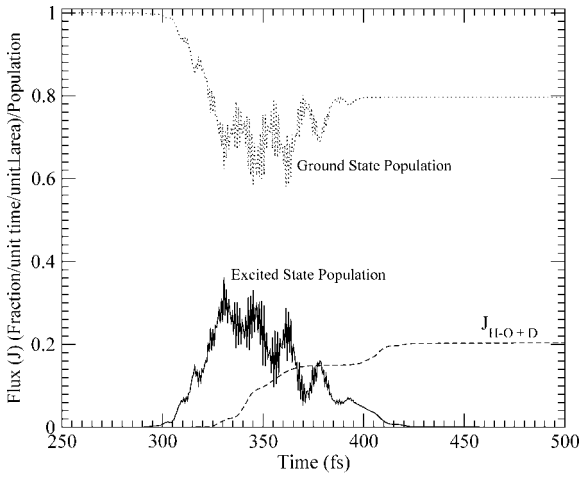

Figure 13. Same as Figures 9 and 11 except $\omega_{uv} = 40\,062$ cm^{-1}.

ground surface, and the population transferred to the excited surface is locked into the H−O + D channel at all times with no flow in the H + O−D channel at any time.

Further lowering of the UV frequency makes the UV pulse off-resonance vis-à-vis the excited surface with insignificant overall dissociation (see Table 2). It can also be seen from Table 2 that as the UV frequency values go beyond 46 062 cm^{-1}, the population transfer on the upper surface will be above the saddle-point barrier, and as expected, there is a loss in selectivity even with this combination of pure O−D modes.

4. Concluding Remarks

We have presented results from a quantum dynamical full two-surface calculation on the HOD molecule to show that the use of a simple IR pulse tuned to the fundamental frequency of the O−H/O−D bond followed by a UV pulse with a carrier

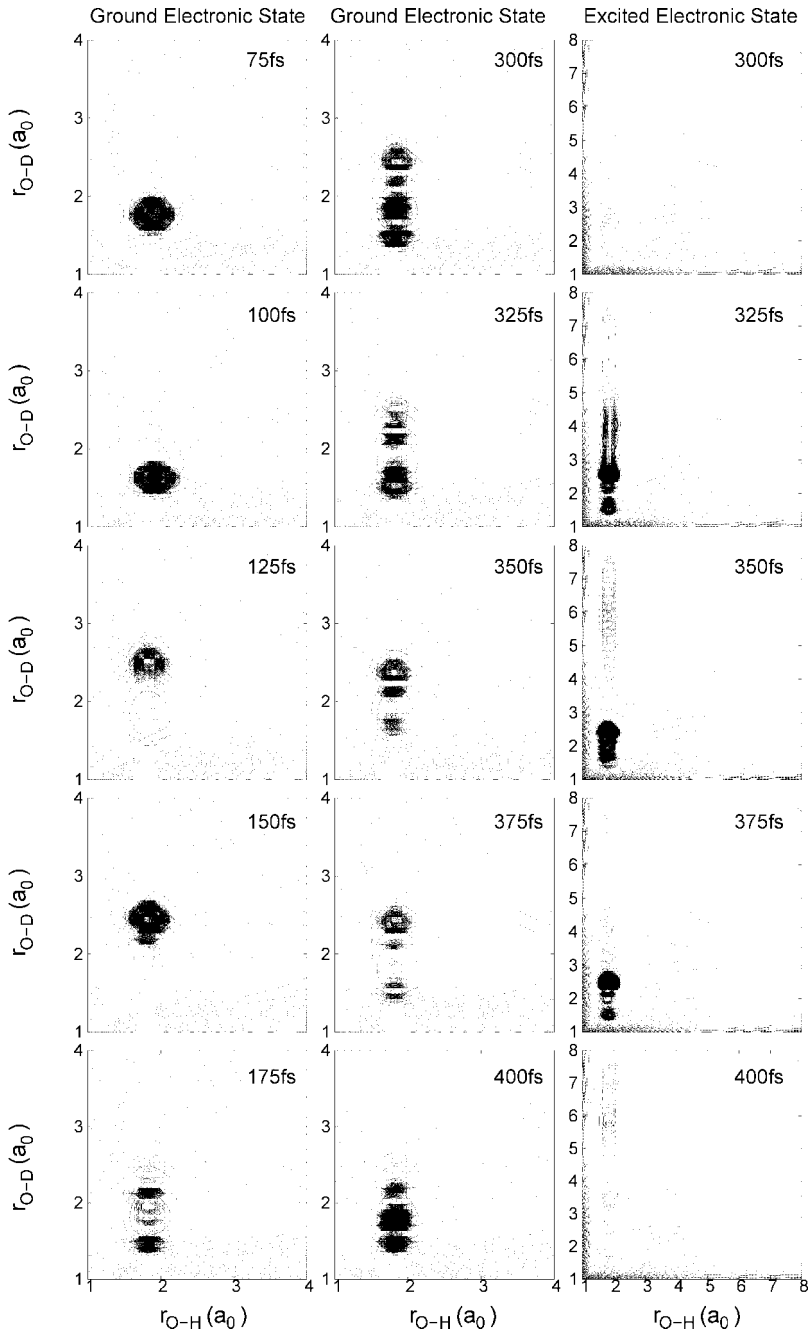

Figure 14. Same as Figures 10 and 12 except $\omega_{uv} = 40\,062$ cm^{-1}.

frequency that deposits the resulting linear combination of pure O−H/O−D modes below the saddle-point barrier can provide an effective pathway for selective dissociation of the desired bond. The dominant stretching mode in the linear combination resulting from the vibrational churn determines the optimal carrier frequency of the UV pulse for maximum yield with reasonable selectivity, which is found to be just enough to deposit the HOD molecule near the saddle point on the repulsive excited surface. Systematic lowering of this carrier frequency gives rise to greater selectivity with reasonable yield, and further lowering gives rise to near total selectivity with reduced yield. The enhanced selectivity with reduction in UV carrier frequency is linked to modification of the cross-talk between the ground and excited surfaces in a manner which removes trans-modal leakage in the competing channel and keeps the population transferred to the upper surface from going over the saddle-point barrier separating the two channels.

A detailed analysis based on examination of population transfer, flux, and probability density flows on the ground and excited surfaces has been employed to corroborate the micro-dynamical quantal picture summarized above.

The successful IR fingerprinting of large molecules buttresses a diatom in the molecule picture, and even phenomena such as single-strand break, double-strand break, and multiple double-strand break in e-DNA scattering[40–47] are being explained as resulting from stretching of individualized bonds. The same individualized bond picture in many cases may therefore probably also permit a vibrational churn of only the bond to be selectively dissociated. Prior churn of the chosen bond by using a sufficiently intense IR laser tuned to its fundamental frequency followed by a calibrated sampling of the effect of a short UV pulse tuned to a repulsive upper surface calculated only for this stretch could provide new insights in selective control of bond dissociation. We therefore feel that the strategy and theoretical tools discussed here could be useful for selective control of bond cleavage in other systems as well, and an effort along these lines is underway in our group.

Acknowledgment. This research has been supported by grants from the Department of Science and Technology (DST) (Grant no. SR/S1/PC-30/2006) and Board of Research in Nuclear Sciences of the Department of Atomic Energy, India, M.K.M. M.S. acknowledges support from CSIR, India (SRF, F. no. 9/87(336)/2003-EMR-I).

References and Notes

(1) Chakrabarti, R.; Rabitz, H. *Int. Rev. Phys. Chem.* **2007**, *26*, 671.
(2) Rabitz, H. *Science* **2006**, *314*, 264.
(3) Shapiro, M.; Brumer, P. *Phys. Rep.* **2006**, *425*, 195.
(4) Shapiro, M.; Brumer, P. *Principles of the Quantum Control of Molecular Processes*; Wiley: New York, 2003.
(5) Henriksen, N. E. *Chem. Soc. Rev.* **2002**, *31*, 37.
(6) Rice, S. A. *Nature* **2001**, *409*, 422.
(7) Rice, S. A.; Zhao, M. *Optical Control of Molecular Dynamics*; Wiley: New York, 2000.
(8) Segev, E.; Shapiro, M. *J. Chem. Phys.* **1982**, *77*, 5604.
(9) Engel, V.; Schinke, R. *J. Chem. Phys.* **1988**, *88*, 6831.
(10) Zhang, J.; Imre, D. G. *Chem. Phys. Lett.* **1988**, *149*, 233.
(11) Zhang, J.; Imre, D. G.; Frederick, J. H. *J. Phys. Chem.* **1989**, *93*, 1840.
(12) Shafer, N.; Satyapal, S.; Bershon, R. *J. Chem. Phys.* **1989**, *90*, 6807.
(13) Imre, D. G.; Zhang, J. *Chem. Phys.* **1989**, *139*, 89.
(14) Hartke, B.; Manz, J.; Mathis, J. *Chem. Phys.* **1989**, *139*, 123.
(15) Vander Wal, R. L.; Scott, J. L.; Crim, F. F. *J. Chem. Phys.* **1990**, *92*, 803.
(16) Bar, I.; Cohen, Y.; David, D.; Rosenwaks, S.; Valentini, J. J. *J. Chem. Phys.* **1990**, *93*, 2146.
(17) Vander Wal, R. L.; Scott, J. L.; Crim, F. F.; Weide, K.; Schinke, R. *J. Chem. Phys.* **1991**, *94*, 3548.
(18) Bar, I.; Cohen, Y.; David, D.; Arusi-Parper, T.; Rosenwaks, S.; Valentini, J. J. *J. Chem. Phys.* **1991**, *95*, 3341.
(19) Amstrup, B.; Henriksen, N. E. *J. Chem. Phys.* **1992**, *97*, 8285.
(20) Shapiro, M.; Brumer, P. *J. Chem. Phys.* **1993**, *98*, 201.
(21) Henriksen, N. E.; Amstrup, B. *Chem. Phys. Lett.* **1993**, *213*, 65.
(22) Cohen, Y.; Bar, I.; Rosenwaks, S. *J. Chem. Phys.* **1995**, *102*, 3612.
(23) Brouard, M.; Langford, S. R. *J. Chem. Phys.* **1997**, *106*, 6354.
(24) Campolieti, G.; Brumer, P. *J. Chem. Phys.* **1997**, *107*, 791.
(25) Meyer, S.; Engel, V. *J. Phys. Chem. A* **1997**, *101*, 7749.
(26) Elghobashi, N.; Krause, P.; Manz, J.; Oppel, M. *Phys. Chem. Chem. Phys.* **2003**, *5*, 4806.
(27) Henriksen, N. E.; Møller, K. B.; Engel, V. *J. Chem. Phys.* **2005**, *122*, 204320.
(28) Akagi, H.; Fukazawa, H.; Yokoyama, K.; Yokoyama, A. *J. Chem. Phys.* **2005**, *123*, 184305.
(29) Møller, K. B.; Westtoft, H. C.; Henriksen, N. E. *Chem. Phys. Lett.* **2006**, *419*, 65.
(30) Sarma, M.; Adhikari, S.; Mishra, M. K. *Chem. Phys. Lett.* **2006**, *420*, 321.
(31) Adhikari, S.; Deshpande, S.; Sarma, M.; Kurkal, V.; Mishra, M. K. *Radiat. Phys. Chem.* **2006**, *75*, 2106.
(32) Sarma, M.; Adhikari, S.; Mishra, M. K. *J. Chem. Phys.* **2007**, *127*, 024305.
(33) Manz, J.; Paramonov, G. K. *J. Phys. Chem.* **1993**, *97*, 12625.
(34) Engel, V.; Schinke, R.; Staemmler, V. *J. Chem. Phys.* **1988**, *88*, 129.
(35) Reimers, J. R.; Watts, R. O. *Mol. Phys.* **1984**, *52*, 357.
(36) Staemmler, V.; Palma, A. *Chem. Phys.* **1985**, *93*, 63.
(37) Dutta, P.; Adhikari, S.; Bhattacharyya, S. P. *Chem. Phys. Lett.* **1993**, *212*, 677.
(38) Kosloff, D.; Kosloff, R. *J. Comput. Phys.* **1983**, *52*, 35.
(39) Leforestier, C.; Bisseling, R. H.; Cerjan, C.; Feit, M. D.; Friesner, R.; Guldberg, A.; Hammerich, A.; Jolicard, G.; Karrlein, W.; Meyer, H. -D.; Lipkin, N.; Roncero, O.; Kosloff, R. *J. Comput. Phys.* **1991**, *94*, 59.
(40) Boudaïffa, B.; Cloutier, P.; Hunting, D.; Huels, M. A.; Sanche, L. *Science* **2000**, *287*, 1658.
(41) Barrios, R.; Skurski, P.; Simons, J. *J. Phys. Chem. B* **2002**, *106*, 7991.
(42) Huels, M. A.; Boudaïffa, B.; Cloutier, P.; Hunting, D.; Sanche, L. *J. Am. Chem. Soc.* **2003**, *125*, 4467.
(43) Li, X.; Sevilla, M. D.; Sanche, L. *J. Am. Chem. Soc.* **2003**, *125*, 13668.
(44) Scheer, A. M.; Aflatooni, K.; Gallup, G. A.; Burrow, P. D. *Phys. Rev. Lett.* **2004**, *92*, 068102.
(45) Berdys, J.; Anusiewicz, I.; Skurski, P.; Simons, J. *J. Am. Chem. Soc.* **2004**, *126*, 6441.
(46) Martin, F.; Burrow, P. D.; Cai, Z.; Cloutier, P.; Hunting, D.; Sanche, L. *Phys. Rev. Lett.* **2004**, *93*, 068101.
(47) Simons, J. *Acc. Chem. Res.* **2006**, *39*, 772.

JP711984T